Light Metals 2011 *Edited by: Stephen J. Lindsay*
TMS (The Minerals, Metals & Materials Society), 2011

Evaluation of thermophysical properties of silicon carbide, graphitic and graphitized carbon sidewall lining materials used in aluminium reduction cell in function of temperature

Ayesha Khatun, Martin Désilets
LAPSUS (Laboratoire des Procédés industriels et Simulations numériques de l'Université de Sherbrooke) Université de Sherbrooke
2500 Boul. de l'Université, Sherbrooke, Québec, J1K 2R1, Canada

Keywords: Thermal conductivity, Thermal diffusivity, Heat capacity, Temperature varying properties, Sidewall lining material.

Abstract

The thermal properties of the sidewall lining materials are required to ensure good predictions of the dynamic thermal behavior of Hall-Heroult cells. A precise estimation of energy losses and location of the side freeze are made possible when these materials are well characterized as a function of temperature. The present work uses transient characterization techniques to measure the thermal diffusivity, heat capacity and thermal conductivity of silicon carbide, graphitic and graphitized carbon materials. The thermal diffusivity and the heat capacity are measured using a state-of-the-art transient laser flash analyzer and a differential scanning calorimeter respectively. The thermal conductivity is calculated by assuming a constant density. Finally, based on the calculations conducted with a 2-D numerical model, the effect of the temperature varying thermal properties of the sidewall materials on the dynamic behavior of a laboratory scale phase change reactor is presented.

Introduction

Generally, the carbon materials used in cathodes are also used for the sidelining of aluminium pots [1]. Sidewalls made of graphitic carbon are losing interest because of their lower resistance to air oxidation and chemical corrosion. The molten metal and corrosive electrolytic bath deteriorate graphitic carbon easily and rapidly which leads to higher risk of sidewall failure and shorter cell life [2]. Graphite has better thermal properties than graphitic material. However, at cell operating temperature, graphite can also be oxidized to CO_2. Nowadays, ceramic sidewall lining material like silicon carbide is typically used for the construction of the sidewall of the aluminium cell due to its high chemical resistivity and its excellent thermal conductivity. It can withstand the extremely corrosive molten electrolyte for long periods [3].

The thermal properties of sidewall lining material have a significant impact on the thermal equilibrium inside the pot. For instance, a high thermal conductivity helps to maintain the desired amount of ledge protection on the sidewall. In consequence, the thermophysical properties of such materials have a significant effect on the heat losses through the sidewall.

The thermal conductivity of different carbon materials used as cathodes has been measured by Dumas et al. [4], using a direct steady state method named KOLHRAUSCH. This same method has been adapted by Allard et al. [5] using a radial heat flow mode to measure the thermal conductivity of graphitized carbon. Llavona et al. [6] described the different measurement methods to determine the thermal properties of materials like insulation, refractories, ceramics, etc., used in industrial aluminium cells. They described the limitations of the steady state method and focused on the use of transient methods to measure the thermal properties. In steady state methods, a massive sample cylinder is typically required which introduces significant temperature variations during the measurements. Also, the heat losses through the thermocouples are source of errors during the measurement. Finally, the development of a steady state experimental setup and the measurement operation are lengthy and time consuming [6].

To overcome these limitations, the present work aims at using transient methods for measuring the thermal properties of three different sidewall materials. In combination with computerized data processing, such techniques can produce accurate and reliable data from room temperature to high temperatures for all types of materials [6]. The methods used lead to the measurement of heat capacity and thermal diffusivity in order to calculate the thermal conductivity. In the current work, the density of each sidewall material has been taken from the literature and assumed to be temperature independent. Two cutting edge measurement techniques, Laser Flash Analyzer (LFA) and Differential Scanning Calorimeter (DSC), have been used to measure respectively the thermal diffusivity and heat capacity.

An empirical correlation for each property has also been derived by fitting the measured data with polynomial equations. These equations can be directly used by modelers to calculate the sidewall properties during the estimation of the heat losses and side ledge formation.

This paper also discusses the effect of the sidewall materials on the prediction of the static and dynamic behaviour of the ledge in a laboratory scale phase change reactor. This physical model of an aluminium electrolysis cell represents the cooling of liquid electrolytic bath inside a crucible made out of industrial sidewall materials.

Measurement of thermal properties

Thermal diffusivity

The principle of the laser flash method (Figure 1) is based on the heating of a specimen by a short laser pulse on its front side and the detection of the temperature increase at its rear side. The thermal diffusivity is determined based on the relative temperature change as a function of time only.

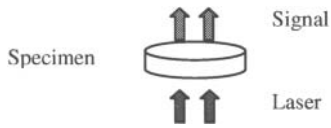

Figure 1: Laser applied at the front side of the specimen.

The thermal diffusivity α is calculated according to equation (1), where d is the thickness of the sample and $t_{½}$ is the time taken to reach half of the temperature increase due to the laser pulse [7]:

$$\alpha = 0.1388\frac{d^2}{t_{\frac{1}{2}}} \quad (1)$$

This equation is based on the following assumptions:

- the laser energy is applied instantaneously i.e. the heat pulse duration is negligible,
- there is no heat loss from the side of the sample,
- heat conduction in the sample is one dimensional and unsteady.

The sample specimen was prepared by machining the material into a long cylinder by using a lathe machine. The desired sample thickness is then obtained by using a diamond saw. A special care has been given on the sample dimensions, sample surface finishing and surface blackness. These parameters play a vital role for obtaining good thermal diffusivities. The sample surface should be smooth enough and plane parallel. Its color should be as black as possible. Smooth and black surfaces give good signal responses and good absorption of the laser energy.

The sample diameter should be within 12.66 to 12.68 mm to fit the sample holder of the Netzsch LFA model 457 used for the measurement of the thermal diffusivities. This range of diameters prevents the direct penetration of laser at the rear surface of the sample. The sample thickness has been chosen according to the rules of thumb suggested by the manufacturer of the equipment [8].

Thermal diffusivity values have been measured in a 25 to 1000 °C temperature range for three different thicknesses at the same time. The optimum thickness has been chosen based on the following criteria:

- Good signal versus time curve provided by the detector.
- Good matching of the thermal conductivity values with the literature values already reported for similar materials, as the thermal diffusivity values of the specific materials studied here are not available in the open literature.

Heat capacity

The heat capacity of each sample has been measured by using a transient relative method called Differential Scanning Calorimetry (DSC). This cutting edge technology can measure two quantities at the same time, the heat flow rate and the corresponding ΔT between a sample and a reference material. This measurement is usually accomplished in three steps - baseline measurement, sample measurement and reference measurement. The most important factors to get precise measurements with this method are to maintain a good contact between the sample and the crucible surface and to use a sample of cylindrical shape. It is also essential to have plane and smooth surfaces.

A standard diameter of 5±0.2 mm is required to avoid the direct contact of the sample with the inner sidewall of the crucible while measuring the heat capacity. The standard thickness of the sample is kept to approximately 1 mm. This value however depends on the density and mechanical strength of the sample material at such low thicknesses.

Thermal conductivity

One of the main key parameters in heat conduction is the thermal conductivity. In this paper, the thermal conductivity is measured indirectly. If the thermal diffusivity (α), density (ρ) and heat capacity (C_p) are known, the thermal conductivity (λ), can be estimated from:

$$\lambda = \alpha\, \rho C_p \quad (2)$$

The calculation of the relative error of the thermal conductivity is essentially the sum of the relative errors on α, ρ and C_p:

$$\frac{d\lambda}{\lambda} = \frac{d\alpha}{\alpha} + \frac{dC_p}{C_p} + \frac{d\rho}{\rho} \quad (3)$$

In theory, the density of a material can have a great impact on the thermal conductivity. In practice however, the density of a solid material does not vary much as a function of temperature. For example, sintered bonded silicon carbide has a density of 3160 kg/m^3 at room temperature and 3110 kg/m^3 at 1000 °C [8]. This represents a 1.5 % variation over a fairly large temperature range. Obviously, neglecting such a variation is introducing an error of 1.5 % in our estimation of the thermal conductivity value at high temperature. The analyses conducted in this paper being comparative, the impact of this density variation on the measurement error is the same for all materials. It has thus been neglected.

Results and discussion

Evaluation of the heat capacity in function of temperature

The heat capacity for each material was measured from room temperature to approximately 1000°C. For each material, an increase in heat capacity as a function of temperature is observed. Heat capacity of silicon carbide is gradually increasing by following two linear curves (Figure 2). The heat capacity of silicon carbide is lower than that of graphitic and graphitized carbon. This difference becomes stronger as temperature increases. At high temperature, the heat capacity of silicon carbide is approximately 1.2 times less than the heat capacity of graphitic and graphitized carbon.

Graphitic and graphitized carbons have almost similar heat capacity temperature functions except at high temperature where the two functions behave differently. At high temperature, the heat capacity of graphitic carbon is lower and more stable than the heat capacity of graphitized carbon.

Polynomial expressions have been fitted on the experimental data. Table 1 presents the regression analysis as applied to the heat capacity (Cp) values, previously adimensionalized by dividing each data by the maximum Cp value of the data set.

Table 1: Empirical correlations for the heat capacity of sidewall lining materials.

Name of materials	Empirical correlations	Regression coefficient
Silicon carbide	$C_p = -3 \times 10^{-7}T^2 + 0.0008T + 0.2329$	$r^2_{Cp} = 0.987$
Graphitic carbon	$C_p = -10^{-6}T^2 + 0.0026T - 0.2413$	$r^2_{Cp} = 0.996$
Graphitized carbon	$C_p = -10^{-6}T^2 + 0.0025T - 0.2272$	$r^2_{Cp} = 0.999$

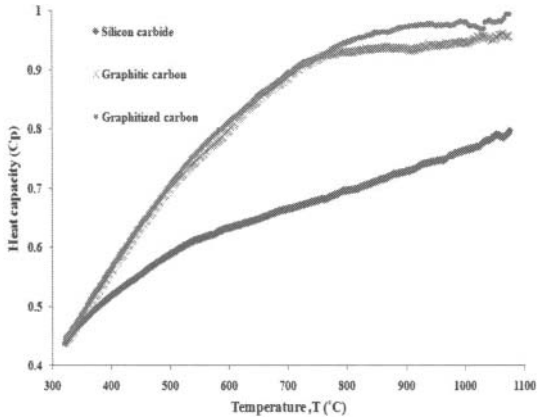

Figure 2: Heat capacity of the sidewall lining materials.

Evaluation of the thermal diffusivity in function of temperature

For each sidewall material, an important decrease in the heat diffusion rate or thermal diffusivity is observed between room and high temperatures (Figure 3). The change of the heat diffusion rate in graphitized carbon is faster than the change observed for graphitic carbon and silicon carbide.

At low temperature, the thermal diffusivity of graphitized carbon is 4.5 times higher than that of silicon carbide (SiC) and 3 times higher than that of graphitic carbon. This difference gradually decreases as temperature increases. At high temperatures, the ratio of thermal diffusivities becomes 2.45 for $\alpha_{graphitized}/\alpha_{graphitic}$ and 2.17 for $\alpha_{graphitized}/\alpha_{SiC}$.

The thermal diffusivity of SiC is higher than the thermal diffusivity of graphitic carbon. However, at high temperature, the thermal diffusivity values of these two materials are very close to each other.

As for the heat capacity, polynomial expressions have been developed (see Table 2) to represent the temperature variation of α/α_{max}, α_{max} being the maximum value of the thermal diffusivity, found here with the graphitized carbon at high temperature.

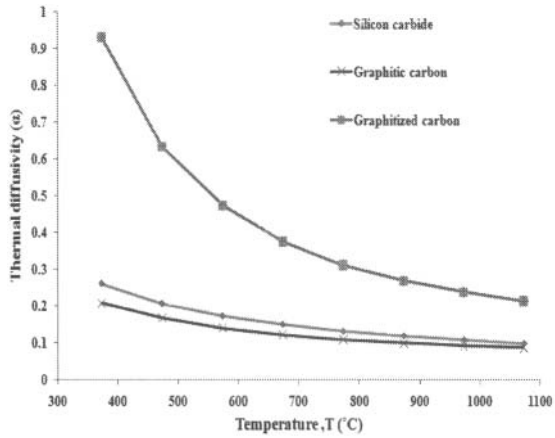

Figure 3: Thermal diffusivity of the sidewall lining materials.

Table 2: Empirical correlations for the thermal diffusivity of sidewall lining materials.

Name of materials	Empirical correlations	Regression coefficient
Silicon carbide	$\alpha = 3 \times 10^{-7}T^2 - 0.0007T + 0.4629$	$r^2_{\alpha} = 0.992$
Graphitic carbon	$\alpha = 3 \times 10^{-7}T^2 - 0.0005T + 0.3676$	$r^2_{\alpha} = 0.992$
Graphitized carbon	$\alpha = 2 \times 10^{-6}T^2 - 0.0037T + 1.996$	$r^2_{\alpha} = 0.980$

Evaluation of the thermal conductivity in function of temperature

While the thermal conductivity of graphitized carbon and SiC gradually decrease with temperature, the thermal conductivity of graphitic carbon is nearly constant (Figure 4).

Initially, the thermal conductivity of graphitized carbon is 5 times higher than that of graphitic carbon and 2.4 times higher than that of SiC. At high temperature, the thermal conductivity of each material is becoming very close to each other, a similar conclusion drawn by Dumas et al. [4] for the thermal conductivity of graphitic and graphitized carbon.

Finally, Table 3 presents the empirical correlations obtained by conducting a polynomial regression on the adimensionalized values of the thermal conductivities.

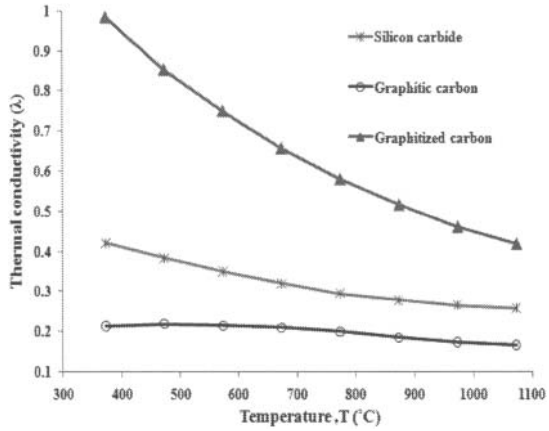

Figure 4: Thermal conductivity of sidewall lining materials.

Table 3: Empirical correlations for the thermal conductivity of sidewall lining materials.

Name of materials	Empirical correlations	Regression coefficient
Silicon carbide	$\lambda = 3 \times 10^{-7}T^2 - 0.0006T + 0.6132$	$r_\lambda^2 = 0.999$
Graphitic carbon	$\lambda = -1 \times 10^{-7}T^2 + 1 \times 10^{-4}T + 0.1971$	$r_\lambda^2 = 0.975$
Graphitized carbon	$\lambda = 7 \times 10^{-7}T^2 - 0.0018T + 1.5413$	$r_\lambda^2 = 0.999$

Effect of the sidewall materials' thermal conductivity on the formation of the ledge

A 2D transient mathematical model in axisymmetric coordinate, similar to the one derived by Marois et al. [9], has been developed to study the effect of the crucible material on the formation of ledge and on the distribution of heat losses inside an experimental phase change reactor. The phase change phenomena has been characterized by simulating the 2D Stefan phase change problem taking into account the latent heat evolution by using an enthalpic formulation. The impact of the thermal properties on the prediction of the ledge profile and on the thermal balance is analyzed based on the numerical results obtained by the mathematical model.

The schematic of the cylindrical shape reactor has been described in figure 5. The sidewall of the reactor is made out of an insulation package. The bottom of the experimental setup is built up from firebricks and castable concrete. The simulation was carried out to predict the dynamic behaviour of the ledge when SiC, graphitic and graphitized carbon are respectively used as the crucible material. The dimensions of the crucible were kept constant for all simulations.

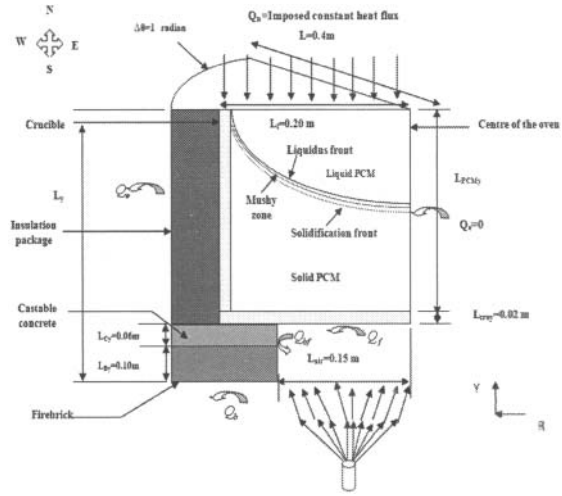

Figure 5: Schematic of the phase change reactor.

To simulate the operation of the oven, a constant heat flux of 20 kW/m^2 is applied at the top of the crucible and of the liquid electrolytic bath, used here as our Phase Change Material (PCM). The bath is numerically solidified in the crucible by extracting the heat through a forced convection air stream applied at the exposed bottom surface of the crucible. The constant forced convection heat transfer coefficient at the bottom of the crucible was calculated as 53 W/m^2/K, based on empirical correlations [10] obtained for similar configuration. The heat loss through the inner exposed surface of the firebrick and castable concrete is also due to this forced convection. The calculated free convection heat transfer coefficient was estimated at 2.6 W/m^2/K for the south west side of the reactor and at 5.86 W/m^2/K for the west side exposed surface of the insulation package. These boundary conditions were kept constant in the evaluation of each crucible material. Starting from an initial condition where the electrolytic bath is liquid, the solidification gradually occurs due to the heat losses from the reactor to the ambient environment through these convective boundaries.

In the numerical simulations, the temperature varying thermal properties (heat capacity and thermal conductivity) of the each sidewall lining material has been taken into account by using the empirical correlations described in tables 1 to 3. The thermal properties of the other materials like firebrick or castable concrete, were determined based on manufacturers' technical data.

The effect of the sidewall materials' thermal properties on the thickness of the ledge is very interesting. As expected, the ledge thickness directly depends on the thermal conductivity of the sidewall materials. The global effect can be easily explained by representing the one-dimensional heat flow between liquid electrolytic bath and ambient environment (Figure 6), using the electrical network analogy. The thermal resistance due to the convection heat transfer outside of the reactor and the global temperature difference (ΔT) between the reactor and the ambient air are considered constant in our analysis. The higher is the thermal conductivity of the sidewall, the lower is the thermal resistance in the crucible region. The constant heat flux entering at

the top of the crucible and liquid electrolytic bath can be expressed as:

$$Q_n = \frac{\Delta T}{R_{tot}} \quad (4)$$

Where $$R_{tot} = R_b + R_c + R_{amb} \quad (5)$$

R_b= thermal resistance of the bath zone, essentially due to solidified bath,

R_c= thermal resistance of the crucible,

R_{amb}= thermal resistance due to convection to the environment.

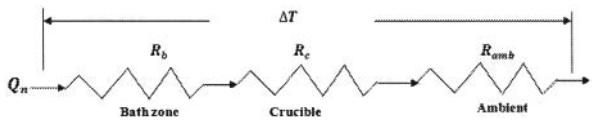

Figure 6: Thermal resistance network representing one dimensional heat flow between the liquid electrolytic bath and the ambient environment.

The only way to keep Q_n constant when ΔT is constant, is to keep R_{tot} constant. When a crucible material of higher thermal conductivity is used, R_c is expected to be lower. Thus R_b will have to compensate the reduction of R_c by forming more ledge on the inside bottom surface of the crucible. When the thermal conductivity of crucible material is low, the reverse phenomenon will be observed.

The ledge formed in the graphitized carbon crucible is the thickest one as this material is introducing the lowest resistance in the thermal resistance network. For the same reason, the ledge is thicker in the SiC crucible than the one formed in graphitic carbon. At steady state conditions, the thickness of the ledge formed at the center of the graphitic carbon and silicon carbide crucible are almost identical, whereas the ledge formed at the center of the graphitized carbon crucible is about 0.5 cm thicker (Figure 7). The difference between the behaviour of these materials is best seen at the peripheral regions of the crucible. The system goes to steady state conditions more slowly when graphitized carbon is used; the additional ledge formed causing an inertial effect on the thermal system. At steady state conditions, the power losses through the exposed bottom surface is boosted up by 4.2 % for the graphitized crucible and by 1.3 % for the SiC crucible when compared to graphitic carbon (Table 4).

The dynamic behavior of the reactor has also been evaluated for each of the crucibles. The simulations have been conducted up to the steady state condition of the system. As explained above, the movement of the ledge in the upward direction is slower in the graphitized crucible (Figure 8). The moving rates of the solidification front in silicon carbide and graphitic carbon crucible are very close to each other (Figure 9 and 10). However, at steady state conditions, more ledge is formed in the SiC crucible than in the graphitic carbon crucible.

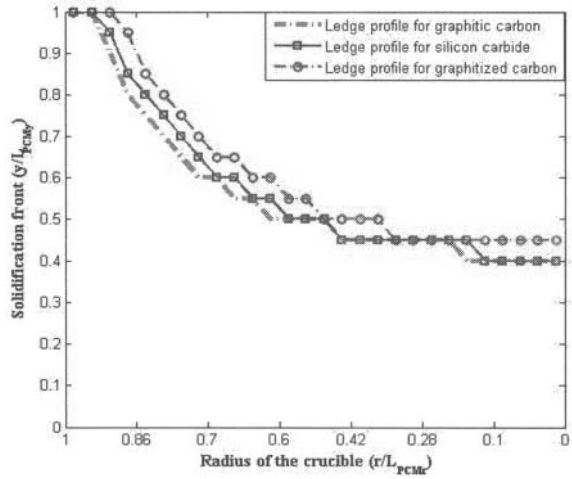

Figure 7: Effect of sidewall materials' thermal conductivity on the prediction of the steady state profile of ledge.

Table 4: Power losses in the reactor for different crucible materials.

Crucible	South side exposed bottom surface of the crucible, (W)	Percentage of variation with respect to graphitic carbon
Graphitic carbon	1325.6	-
Silicon carbide	1342.4	1.3 %
Graphitized carbon	1381.3	4.2 %

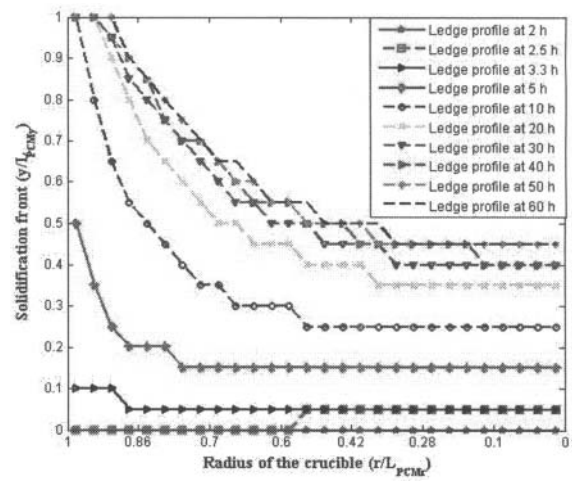

Figure 8: Dynamic behaviour of the ledge formed after starting the cooling process of liquid electrolytic bath in the graphitized crucible.

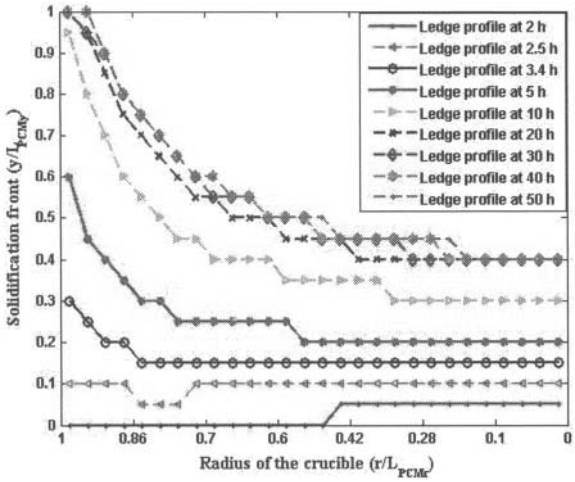

Figure 9: Dynamic behaviour of the ledge formed after starting the cooling process of liquid electrolytic bath in the silicon carbide crucible.

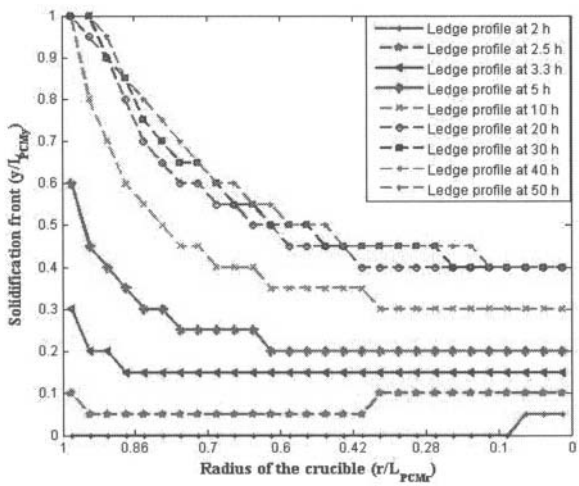

Figure 10: Dynamic behaviour of the ledge formed after starting the cooling process of liquid electrolytic bath in the graphitic crucible.

Conclusions

The presented research work aims at the precise measurement of the thermal properties of graphitic and graphitized carbon and silicon carbide sidewall lining materials used in the aluminium reduction cell. The heat capacity and the thermal diffusivity of each material have been measured and used to estimate the thermal conductivity at constant density. The effect of the thermal conductivity of the each sidewall material on the prediction of the bottom ledge inside a laboratory scale phase change reactor has also been estimated by using the empirical correlation derived by using polynomial fitting of the estimated thermal conductivity.

As expected, graphitized carbon has the highest thermal conductivity in comparison to the other sidewall lining material evaluated. When graphitized carbon sidewall is used, the ledge formed at the steady state conditions is the thickest one, followed by the silicon carbide and by the graphitic carbon. The thermal conductivity of the material used for the sidewall construction significantly affects the side ledge thickness over it, especially during the transient conditions. These variations in ledge thickness also lead to variations of the sidewall heat losses.

Acknowledgements

The authors are grateful to Rio Tinto Alcan for their financial support.

References

[1] Sørlie, Morten. and Øye, Harald A (1994). Cathodes in aluminium electrolysis, 2nd edition, Aluminium –Verlag, 1994, p. 12-23.

[2] Boily, P., Kiss, L.I., Bui, R.T. and Desclaux, P. (2001). Sensitivity analysis of the thermal detection of the Ledge profile in an aluminium reduction cell. Light Metals 2001, p. 1209.

[3] Pan, Yuhua., Wright, Steven. and Sun, Shouyi (2009). Review and applications of thermal conductivity models to aluminium cell sidewall refractories. International Journal of Modern Physics B. Vol. 23, Nos. 6 & 7 (2009), p.790.

[4] Dumas, D. and Lacroix, P. (1994). High temperature measurement of electrical resistivity and thermal conductivity on carbon materials used in aluminium smelters, Light Metals, 1994, p. 751.

[5] Allard, Benedict. Dreyfus, Jean-Michel. and Lenclud, Michel (2000). Evolution of thermal, electrical and mechanical properties of graphitized cathode blocks for aluminium electrolysis cells with temperatures, Light Metals, 2000, p. 515.

[6] Llavona, M.A., MaAyala, J., García, MaP., Zapico, R. and Sancho, J.P. Thermal conductivity measurement of the materials in the aluminium industry, Light Metals 1994, p.467.

[7] Laser flash analyzer instrument Manual provided by Netzsch.

[8] http://www.ceramics.nist.gov/srd/summary/scdscs.htm, NIST, Property Data Summaries, page consulted at 13 September 2010.

[9] Marois, M., Bertrand, C., Desilets, M., Coulombe, M and Lacroix, M (2009). Comparison of two different numerical methods for predicting the formation of the side ledge in aluminium electrolysis cell, Light Metals, 2009, p. 563.

[10] Incropera, Frank P., Dewitt, David P., Bergman, Theodore and Lavine, Adrienne S. Introduction to Heat Transfer, 6th edition, Chapter 7, John Wiley & Sons, Inc, P. 423-428,431.